Mean-field behavior of the negative-weight percolation model on random regular graphs

Oliver Melchert* and Alexander K. Hartmann
Institute of Physics, University of Oldenburg, 26111 Oldenburg, Germany

Marc Mézard
Laboratoire de Physique Théorique et Modeles Statistiques, Université de Paris Sud, 91405 Orsay, France
(Dated: July 27, 2012)

We investigate both analytically and numerically the ensemble of minimum-weight loops and paths in the negative-weight percolation model on random graphs with fixed connectivity and bimodal weight distribution. This allows us to study the mean-field behavior of this model. The analytical study is based on a conjectured equivalence with the problem of self-avoiding walks in a random medium. The numerical study is based on a mapping to a standard minimum-weight matching problem for which fast algorithms exist. Both approaches yield results which are in agreement, on the location of the phase transition, on the value of critical exponents, and on the absence of any sizeable indications of a glass phase. By these results, the previously conjectured upper critical dimension of $d_u = 6$ is confirmed.

PACS numbers:

I. INTRODUCTION

The statistical properties of lattice-path models on graphs, equipped with quenched disorder, have experienced much attention during the last decades. They have proven to be useful in order to describe line-like quantities as, e.g., linear polymers in disordered media [1–4], vortices in high T_c superconductivity [5, 6], cosmic strings in the early universe [7–9], and domain-wall excitations in disordered systems such as $2d$ spin glasses [10, 11] and the $2d$ solid-on-solid model [12]. The precise computation of these paths can often be formulated in terms of a combinatorial optimization problem and hence might allow for the application of exact optimization algorithms developed in computer science [13–15]. So as to analyze the statistical properties of these lattice path models, geometric observables and scaling concepts similar to those used in percolation theory [16, 17] or other "string"-bearing models [18, 19] are often applicable.

This paper studies the *negative-weight percolation* (NWP) problem [20–22], wherein one considers a graph where sites are joined by undirected edges. Weights are assigned to the edges, representing quenched random variables drawn from a distribution that allows for edge weights of either sign. The details of the weight distribution are further controlled by a tunable disorder parameter. We are interested in configurations consisting of one path and a set of loops, i.e. closed paths on the graph, such that the total sum of the weights assigned to the edges that build up the path and the loops attains a minimum. We will study here the mean-field behavior of this model by means of numerical simulations and analytical studies on random regular graphs. For the numerical studies, one could use standard sampling approaches like Monte Carlo simulations but they exhibit the usual equilibration problems. Fortunately, one can map NWP to the standard minimum-weight perfect matching optimization problem, as outlined below in sect. II in more detail. This mapping allows to apply exact polynomial-time-running algorithms. Thus, large instances can be solved. As an additional optimization constraint we impose the condition that the string-like observables (referring to both, the loops and the path) are not allowed to intersect. Consequently, since a string-like observable does neither intersect with itself nor with other strings in its neighborhood, it exhibits an "excluded volume" quite similar to usual self avoiding walks (SAWs) [17]. We shall develop in this paper the analogy between SAWs and NWP, and use some of the recently developed tools in the studies of polymers on random graphs in order to derive an analytical study of the NWP problem.

As presented here, the NWP problem is a theoretical model of intrinsic interest. As an example that makes use of the NWP problem statement one can imagine an agent that travels on a graph. While traversing an edge, the agent either needs to pay some resource (signified by a positive edge weight) or he is able, once per edge, to harvest some resource (signified by a negative edge weight). Now, if the intention of the agent is to gain as much resources as possible, the paths/loops obtained in the context of the NWP problem can serve as a guide to find routes along which the agent might move so as to optimize his yield. Further, the 2d variant of the NWP problem is interesting from a technical and algorithmic point of view. As regards this, the problem of finding ground-state spin configurations for the $2d$ random-bond Ising model, including the canonical Ising spin glass, on a planar triangular lattice can be mapped to the 2d NWP problem on a honeycomb lattice [23, 24] (Analogous to the approach presented in [25, 26], the basic idea of this

*Electronic address: oliver.melchert@uni-oldenburg.de

mapping is to compute a transition graph that mediates the transformation from an initially chosen reference spin configuration to a proper GS). Moreover, paths that include negative edge-weights also appear in the context of domain wall excitations in $2d$ random bond Ising systems [11, 27]. Thus, the NWP problem might serve to gain insight concerning the behavior of more realistic disordered systems.

Previous studies [20–22] of the NWP model considered regular lattice graphs in dimension d with periodic boundary conditions. As a pivotal observation it was found that, as a function of the disorder parameter, the NWP model features a disorder-driven, geometric phase transition. This transition leads from a phase characterized by only "small" loops to a phase that also features "large" loops that span the entire lattice along at least one direction. Regarding these two phases and in the limit of large system sizes, there is a particular value of the disorder parameter at which percolating (i.e. system spanning) loops appear for the first time [20]. Previously, we have investigated the NWP phenomenon for $2d$ lattice graphs [20] using finite-size scaling (FSS) analyses, where we characterized the underlying transition by means of a whole set of critical exponents. Considering different disorder distributions and lattice geometries, the exponents were found to be universal in $2d$ and clearly distinct from those describing other percolation phenomena. In a subsequent study, we performed further simulations for the NWP model on hypercubic lattice graphs in dimensions $d=2$ through 7 [22], where we aimed to assess the upper critical dimeison d_u of the NWP model. As a fundamental observable that provides information on whether the upper critical dimension d_u is reached, we monitored the fractal dimension d_f of the loops. The fractal dimension can be defined from the scaling of the average length $\langle \ell \rangle$ of the percolating loops as a function of the linear extension L of the lattice graphs, according to $\langle \ell \rangle \sim L^{d_f}$. For $d \geq d_u$ one might expect to observe $d_f = 2$, which signifies the mean-field limit for self-avoiding lattice curves. This means, the "excluded volume" effect mentioned earlier becomes irrelevant and the loops exhibit the same scaling as ordinary random walks. From that study, considering regular d-dimensional lattice graphs, we found evidence for an upper critical dimension $d_u = 6$ for the NWP phenomenon.

To resume, previous works have focused on the critical properties of the NWP model on regular lattice graphs, where the upper critical dimension can be defined as the smallest dimension for which the critical exponents take their mean field values. Here, we perform simulations and analytical calculations for the NWP problem on random graphs with fixed connectivity (see discussion below), where one has direct access to the mean-field exponents that describe the transition. These studies provide further support for the result $d_u = 6$ obtained previously [22]. Furthermore, we examine the structure of the energy landscape of this problem by studying the existence of low-energy excitations involving a finite fraction of the system. The numerical simulations presented here are carried out on the ensemble of random regular graphs with a fixed node degree. Due to the absence of, say, a regular lattice geometry that allows for a clear cut definition of spanning lengths of loops (as it was possible in previous studies), we found it more beneficial to focus on the scaling properties of minimum weight paths instead. In this regard, if we select two nodes on a random graph we can compare the properties of the minimum weight path to the shortest path that connect the two distinguished nodes. In the context of the presented study, this will provide means to assess the scaling properties of the paths. Further, note that in a previous study [20] we verified that loops and paths in the NWP problem give rise to identical scaling properties.

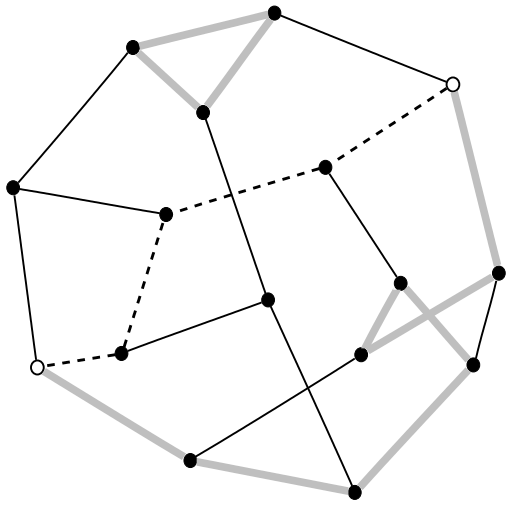

FIG. 1: Example of a r-regular random graph with $N = 16$ nodes and fixed degree $r = 3$. The depicted graph has a diameter $R_{N,r} = 4$, where the diameter is the longest among all shortest paths (measured in node-to-node hops). For a given realization of the quenched disorder, the negative-weight percolation algorithm might yield the path+loop configuration illustrated by means of the bold gray edges. Therein, a path is forced to join two distinguished nodes (open circles) that are maximally seperated, i.e. have distance $R_{N,r}$. The dashed path corresponds to a shortest path joining the two distinguished nodes.

The remainder of the presented article is organized as follows. In section II, we introduce the model in more detail and we outline the algorithm used to compute the minimum weight configurations of loops. In section III, we present the results of our numerical simulations. In section IV, we explain the analytical cavity approach through a mapping to SAWs, and we show the corresponding results. Finally, in section V we conclude with a summary. Note that an extensive summary of this paper is available at the *papercore database* [28].

II. MODEL AND ALGORITHM

In the remainder of this article we consider r-regular random graphs (r-RRGs) $G_{N,r}=(V,E)_{N,r}$, wherein V is a set of N nodes $i\in V$, having fixed degree $\deg(i)=r$. Accordingly, E is a set of $rN/2$ edges $e_{ij}=\{i,j\}$, $i,j\in V$, randomly drawn from $V^{(2)}$ with the restriction that each node has exactly r neighbors. Further, the distance d_{ij} between two nodes $i,j\in V$ is the number of steps in the shortest (i.e. minimum-length) path joining both nodes. If the respective nodes cannot be joined by a path, the distance is taken as infinite. Then, the diameter $R_{N,r}$ of an instance of $G_{N,r}$ is the largest finite distance within the given graph. Further, two nodes $i,j\in V$ satisfying $d_{ij}=R_{N,r}$ are said to be maximally separated. Fig. 1 illustrates an istance of $G_{N,r}$ with $N=16$ and $r=3$. At this point we would like to point out that there exists an intricate relation between the number of nodes and the diameter of r-RRGs. In this regard, early estimates for fixed $r\geq 3$ yield the result that there is a r-RRG of diameter at most $R_{N,r}=\lceil \log_{r-1}((2+\epsilon)N\log(N)/r)\rceil+1$ (where $\epsilon>0$) [29, 30]. Later, it was indicated that the diameter of 3-RRGs scales as $R_{N,3}=1.4722\log(N)+O(1)$ [31]. Further, for $r=4$ the relation $R_{N,4}=0.9083\log(N)+O(1)$ was found [31]. These results also agree with the expression $R_N=c\log(N)+O(\log(N))$ for the diameter of sparse random graphs with specified degree sequence [32]. Subsequently we fix $r=3$ and substitute $R_{N,r}\equiv R_N$ and $G_{N,r}\equiv G$.

We further assign a weight ω_{ij} to each edge contained in E, representing quenched random variables that introduce additional disorder to the random graph ensemble. In the presented article we consider weights that are drawn from the bimodal disorder distribution

$$P(\omega)=\rho\delta(\omega+1)+(1-\rho)\delta(\omega-1)\,. \tag{1}$$

The disorder parameter ρ therein allows to adjust the fraction of negative edge weights on the graph. Note that this disorder distribution explicitly allows for loops $\mathcal{L}$ with a negative total weight $\omega_{\mathcal{L}}=\sum_{\{i,j\}\in\mathcal{L}}\omega_{ij}$. To support intuition: For any nonzero value of the disorder parameter ρ, a sufficiently large graph will exhibit at least "small" loops that have negative weight.

The NWP problem statement then reads as follows: Given G together with a realization of the disorder, determine a set $\mathcal{C}$ of loops such that the configurational energy, defined as the sum of all the loop-weights $\mathcal{E}=\sum_{\mathcal{L}\in\mathcal{C}}\omega_{\mathcal{L}}$, is minimized. As further optimization constraint, the loops are not allowed to intersect and generally, the weight of an individual loop is smaller than zero. Note that $\mathcal{C}$ may also be empty (clearly this is the case for $\rho=0$). Clearly, the configurational energy $\mathcal{E}$ is the quantity subject to optimization and the result of the optimization procedure is a set of loops $\mathcal{C}$, obtained using an appropriate transformation of the original graph as detailed in [33]. So as to identify the edges that constitute the loops for a particular instance of the disorder, we can benefit from a relation between minimum-weight paths (and loops) on G and minimum-weight perfect matchings (MWPM) [23, 34, 35] on the transformed graph. Here, we give a brief description of the algorithmic procedure that yields a minimum-weight set of loops for a given realization of the disorder. Fig. 2 illustrates the 3 basic steps, detailed below:

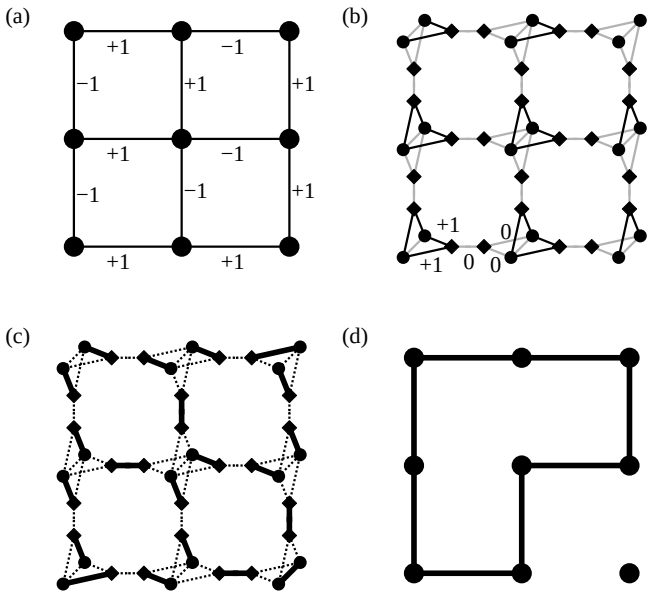

FIG. 2: Illustration of the algorithmic procedure: (a) original lattice G with edge weights, (b) auxiliary graph G_{A} with proper weight assignment. Black edges carry the same weight as the respective edge in the original graph and grey edges carry zero weight, (c) minimum-weight perfect matching (MWPM) M: bold edges are matched and dashed edges are unmatched, and (d) loop configuration (bold edges) that corresponds to the MWPM depicted in (c).

(1) each edge, joining adjacent sites on the original graph G, is replaced by a path of 3 edges. Therefore, 2 "additional" sites have to be introduced for each edge in E. Therein, one of the two edges connecting an additional site to an original site gets the same weight as the corresponding edge in G. The remaining two edges get zero weight. The original sites $i\in V$ are then "duplicated", i.e. $i\to i_1,i_2$, along with all their incident edges and the corresponding weights. For each of these pairs of duplicated sites, one additional edge $\{i_1,i_2\}$ with zero weight is added that connects the two sites i_1 and i_2. The resulting auxiliary graph $G_{\mathrm{A}}=(V_{\mathrm{A}},E_{\mathrm{A}})$ is shown in Fig. 2(b), where additional sites appear as squares and duplicated sites as circles. Fig. 2(b) also illustrates the weight assignment on the transformed graph G_{A}. Note that while the original graph (Fig. 2(a)) is symmetric, the transformed graph (Fig. 2(b)) is not. This is due to the details of the mapping procedure and the particular weight assignment we have chosen. A more extensive description of the mapping can be found in [11].

(2) a MWPM on the auxiliary graph is determined

via exact combinatorial-optimization algorithms [36]. A MWPM is a minimum-weighted subset M of $E_{\rm A}$, such that each site contained in $V_{\rm A}$ is met by precisely one edge in M. This is illustrated in Fig. 2(c), where the solid edges represent M for the given weight assignment. The dashed edges are not matched. Due to construction of the auxiliary graph,

(3) finally it is possible to find a relation between the matched edges M on $G_{\rm A}$ and a configuration of negative-weighted loops $\mathcal{C}$ on G by tracing back the steps of the transformation (1). As regards this, note that each edge contained in M that connects an additional site (square) to a duplicated site (circle) corresponds to an edge on G that is part of a loop, see Fig. 2(d). More precisely, there are always two such edges in M that correspond to one loop segment on G. All the edges in M that connect like sites (i.e. duplicated-duplicated, or additional-additional) carry zero weight and do not contribute to a loop on G. Once the set $\mathcal{C}$ of loops is found, a depth-first search [33, 35] can be used to identify the loop set $\mathcal{C}$ and to determine the geometric properties of the individual loops. For the weight assignment illustrated in Fig. 2(a), there is only one negative weighted loop with $\omega_{\mathcal{L}} = -2$ and length $\ell = 8$.

Note that the result of the calculation is a collection $\mathcal{C}$ of loops such that the total loop weight, and consequently the configurational energy $\mathcal{E}$, is minimized. Hence, one obtains a global collective optimum of the system. Obviously, all loops that contribute to $\mathcal{C}$ possess a negative weight. Also note that the choice of the weight assignment in step (1) is not unique, i.e. there are different possibilities to choose a weight assignment that all result in equivalent sets of matched edges on the transformed lattice, corresponding to the minimum-weight collection of loops on the original lattice. Some of these weight assignments result in a more symmetric transformed graph, see e.g. [33]. However, this is only a technical issue that does not affect the resulting loop configuration. Albeit the transformed graph is not symmetric, the resulting graph (Fig. 2(d)) is again symmetric.

Note that the above description explains how to obtain a set of loops only. If one aims to compute an additional minimum weight path that connects two nodes, say s and t, on the graph, the transformation procedure for these two particular nodes will look slightly different: the duplication step introduced in step (1) will be skipped for nodes s and t, see Fig. 3(a). Computing a MWPM for the resulting graph will then yield a minimum weight path that connects nodes s and t together with a set of loops (the set might be empty) as explained in steps (2) and (3) above. This is illustrated in Fig. 3(b), where for the same weight assignment as in Fig. 2(a), a minimum weight path is computed. For this illustrational purpose, a small $2d$ lattice graph with free BCs was chosen. The algorithmic procedure extends to r-regular random graphs in a straightforward manner.

In the following we will use the procedure outlined above so as to investigate the NWP phenomenon on 3-regular random graphs.

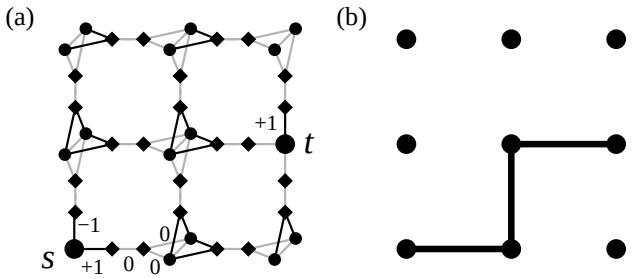

FIG. 3: Illustration of the algorithmic procedure to obtain a minimum weight s-t-path: (a) auxiliary graph $G_{\rm A}$, where the mapping is modified to induce a minimum weight path that connects nodes s and t. Black edges carry the same weight as the respective edge in the original graph and grey edges carry zero weight, (b) minimum weight path (bold edges) that corresponds to a MWPM on $G_{\rm A}$. For the particular example illustrated here, the path has weight $\omega_p = -1$ and there are no loops in addition to the path.

III. RESULTS

In the following we will present the results obtained from numerical simulations of negative weighted loops and paths on 3-regular random graphs.

A. Minimum-weight paths (MWPs)

Once a particular instance of G is constructed and so as to get a grip on the node-to-node distances d_{ij} for $i, j \in V$, we traverse the graph using a depth-first search (DFS) [37]. Invoked to compute the distances from a particular source node to all other nodes in the graph, the DFS terminates in $O(N)$ time. As soon as the DFS is completed for each node in the graph, the diameter of the particular random graph is easily obtained as the largest finite distance in $O(N^2)$ time. Then we compute a minimum weight path on the graph that joins two distinguished nodes $s, t \in V$, satisfying $d_{st} = R_N$. For the range of system sizes considered here, and in qualitative agreement with the $R_N - N$-relation given above, we found the approximate scaling $R_N = 1.68(5)\log(N) + 1.2(5)$, see inset of Fig. 4. As regards this, note that for large graph sizes the diameter does not change much. An increase of $N = 10^3 \to 10^4$ only leads to an increase of $R_N = 13 \to 16.5$. For the scaling behavior of the average length $\langle \ell \rangle$ of the minimum-weight paths we can expect that

$$\langle \ell \rangle \sim \begin{cases} R_N \sim \log(N) & \text{for } \rho \to 0; \\ N & \text{for } \rho \to 1. \end{cases} \qquad (2)$$

This is based on the intuition that as $\rho \to 0$, an increasing path length will lead to an increasing path weight. As a

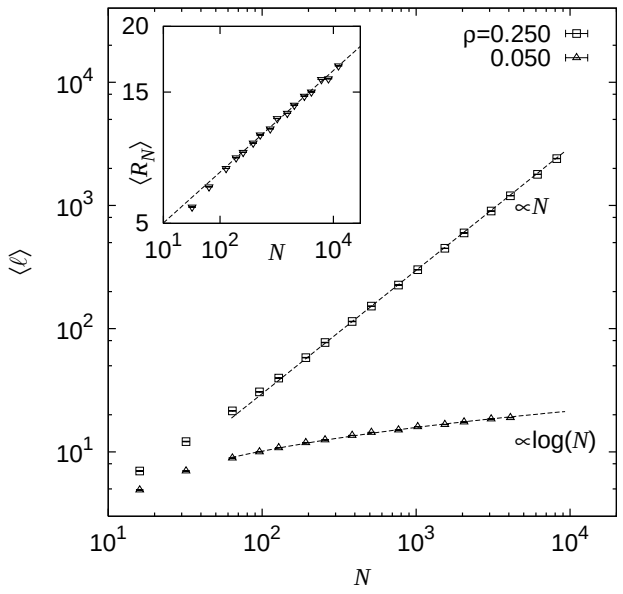

FIG. 4: Scaling behavior of the minimum-weight path length on RRGs respecting a bimodal distribution of the edge-weights. The main plot shows the scaling of the average path length $\langle \ell \rangle$ at the values $\rho = 0.05$ and 0.25 of the disorder parameter, yielding the scaling behavior $\sim \log(N)$ and $\sim N$, respectively. The inset illustrates the scaling of the average RRG diameter as $\langle R_N \rangle \sim 1.68(5) \log(N) + 1.2(5)$ (note that only the x-axis is scaled logarithmically).

result, a minimum weight path that connects two nodes will most likely coincide with the shortest path, i.e. a path using the minimum number of edges. In contrast, as $\rho \to 1$ it becomes feasible to take large detours (relative to the shortest path) so as to traverse many edges with negative weight. Consequently, an increasing path length will result in a decreasing path weight.

Within our simulations we find $\langle \ell \rangle \sim R_N^{1.05(1)}$ at $\rho = 0.04$ and $\langle \ell \rangle \sim N^{0.998(2)}$ at $\rho = 0.25$, in agreement with Eq. 2, see Fig. 4. Here, investigating MWPs on RRGs allows for a direct study of paths in the mean-field setup of the negative-weight percolation model. Now, since R_N is the distance spanned by the MWPs upon construction, we can expect to find the asymptocic scaling behavior $\langle \ell \rangle \sim R_N^2$ at the critical point ρ_c of the setup. This would indicate the same statistical properties as for usual random walks, wherein the directions of consecutive steps along the walk are completely uncorrelated.

B. Bimodal disorder – Path weight

First, we consider the probability $P_N^\omega \equiv P_N(p_\omega \leq 0)$ that the path weight p_ω is smaller/equal to zero. For each realization of the bond disorder, P_N^ω is either 0/1. Hence, for the average value $\langle P_N^\omega \rangle$ we expect a scaling behavior similar to the spanning probability in percolation theory, i.e. $\langle P_N^\omega \rangle \sim f_0[(\rho - \rho_c^\infty) N^{1/\nu^*}]$, wherein $f_0[\cdot]$ is a size-independent scaling function. The value of ρ_c^∞ signifies the location of the critical point, above which, in the limit $N \to \infty$, a path with $p_\omega \leq 0$ appears for the first time. From our simulations we find that with increasing N this crossing point shifts towards smaller values of ρ. This might be attributed to the finite-size of the studied systems and signals corrections to the scaling behavior. So as to account for these corrections to scaling, one may consider an effective scaling expression of the form

$$\langle P_N^\omega \rangle \sim f_1[(\rho - \rho_1(N)) N^{1/\nu_1^*}], \tag{3}$$

wherein $\rho_1(N) = \rho_1^c + a N^{-\phi_1}$. The latter effective scaling form implies 4 adjustable parameters and accounts for a shift in the effective critical point $\rho_1(N)$. Considering Eq. 3, a best data collapse of the curves for $N \geq 1024$ then yields the parameters

$$\begin{aligned} \rho_1^c &= 0.075(1) \\ \phi_1 &= 0.297(7) \\ \nu_1^* &= 3.0(1) \end{aligned}$$

with $a = O(1)$, see Fig. 5(a).

As an alternative, we can estimate the critical point from the location of the maxima of the related finite-size suszeptibilities

$$C_N^\omega = N \langle (P_N^\omega - \langle P_N^\omega \rangle)^2 \rangle = N \mathrm{var}(P_N^\omega). \tag{4}$$

In this regard, if, for a given system size N, the maximum of $\mathrm{var}(P_N^\omega)$ (or similary C_N^ω) is located at the effective critical point $\rho_2(N)$, we expect the sequence of $\rho_2(N)$ for increasing N to approach an asymptotic value of ρ_2^c according to

$$\rho_2(N) = \rho_2^c + a N^{-\phi}. \tag{5}$$

Here, ϕ signifies an effective exponent that accounts for the corrections to scaling in a very basic manner. Note that if there are no corrections to scaling, it holds that $\phi = 1/\nu^*$. The locations $\rho_2(N)$ were obtained by a fit [38] of a gaussian function to the peak of $\mathrm{var}(P_N^\omega)$, as illustrated in Fig. 5(b). The analyisis of $\rho_2(N)$ by means of Eq. 5 for $N \geq 128$, shown in the inset of Fig. 5(b), then yields:

$$\begin{aligned} \rho_2^c &= 0.0758(9) & \qquad \chi^2/\mathrm{dof} &= 0.54 \\ \phi &= 0.288(5) & \qquad \mathrm{dof} &= 3 \end{aligned}$$

Finally, note that the effective scaling form considered here does not properly account for the corrections to the scaling behavior. Actually, a more sophisticated analysis should account for corrections to scaling via $\rho_c(N) = \rho_c^\infty + a(1 + cN^{-\omega}) N^{-1/\nu^*}$. Unfortunately our data did not allow for a more elaborate analysis involving 5 free parameters. However, if we apply the latter scaling form and fix the value of ν^* to the presumably correct value $\nu^* = 3$ we find, again for $N \geq 128$,

$$\begin{aligned} \rho_c^\infty &= 0.077(6) & \qquad \chi^2/\mathrm{dof} &= 0.86 \\ \omega &= 0.06(50) & \qquad \mathrm{dof} &= 2 \end{aligned}$$

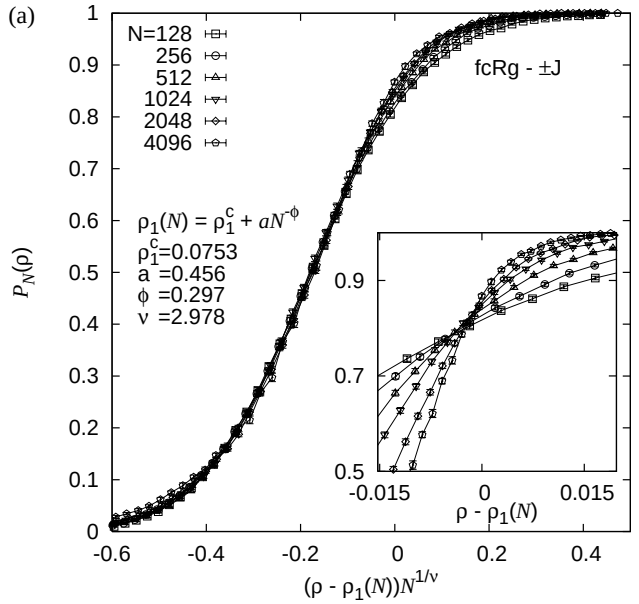

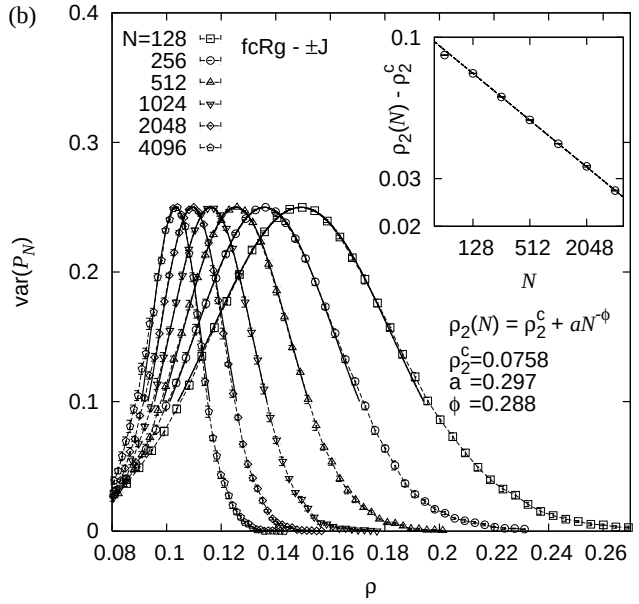

FIG. 5: Results for minimum weight paths on RRGs respecting a bimodal distribution of the edge-weights. (a) Probability $P_N^\omega \equiv P_N(p_\omega \leq 0)$ that a path has negative/zero weight. The main plot shows the rescaled data that also accounts for a drift in the effective critical point $\rho_1(N)$. The inset illustrates the crossing point of the data sets after correcting for the drift. (b) Variance of P_N^ω, related to the finite-size suszeptibility C_N^ω via $C_N^\omega = N\mathrm{var}(P_N^\omega)$. The main plot shows the approximation of the $\mathrm{var}(P_N^\omega)$-peaks by means of fits to a gaussian function. The inset illustrates the the scaling of the peak locations as $\rho_c(N) = \rho_c^\infty + aN^{-\phi}$.

wherein a and c are $O(1)$, and where the values of ρ_c^∞ and ω are in agreement with the values found from the analysis of Eq. 3. Note that the error associated with ω is rather large.

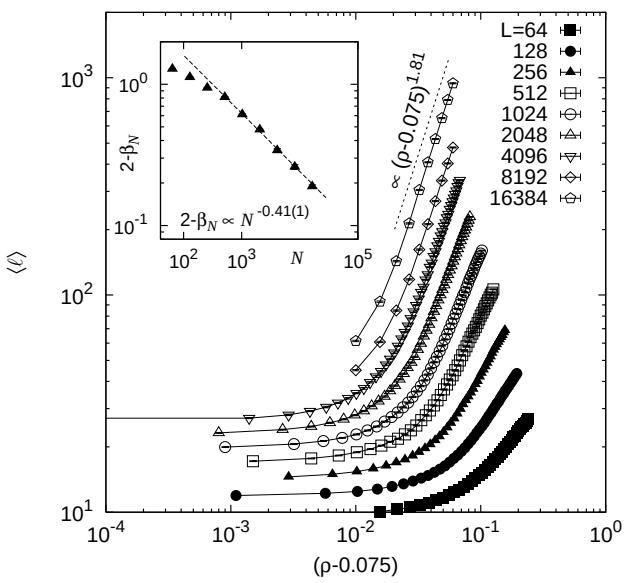

FIG. 6: Scaling of the average path length as a function of the distance to the critical point $\rho_c = 0.075(2)$ for different system sizes N. Not too close to the critical point a power-law behavior is visible. The dashed line shows an exemple of a fit to a power law scaling form $\sim (\rho - \rho_c)^{\beta_N}$, where at $N = 16384$ we find $\beta_N = 1.81(1)$. The inset shows the obtained value $2 - \beta_N$ as a function of system size N. The line shows a power law $\sim N^{-0.41}$. Please note the double logarithmic scales.

From the agreement among the extrapolated results we conclude with a critical point $\rho_c^\infty = 0.075(2)$ and $\nu^* = 3.0(1)$ in agreement with the value $\nu^* = d_c\nu = 3$, that one could expect from the results for the finite-dimensional regular graphs.

Next, we determine the critical exponent β, describing the behavior of the relative path length $\psi = \langle\ell\rangle/N$ as a function on the distance from the critical point according to

$$\psi \sim (\rho - \rho_c)^\beta \,. \tag{6}$$

In Fig. 6, the scaling of $N\psi$ according to Eq. 6 is shown for different values of N. The value of the exponent obtained in the scaling region depends on N, i.e., $\beta = \beta_N$ (for the largest graph size considered, i.e. $N = 16384$, we find $\beta_N = 1.81(1)$). The dependence is well compatible with a finite-size scaling according to $\beta_N = \beta + aN^{-b}$ with $\beta = 2$, $a = 10(1)$, $b = -0.41(1)$, see inset of Fig. 6. Hence, this value of β agrees well with the numerical value $\beta = 1.92(6)$ found [22] for hypercubic lattices at the presumed upper critical dimension $d = 6$. It also agrees with the analytical computation developed in Sect.IV.

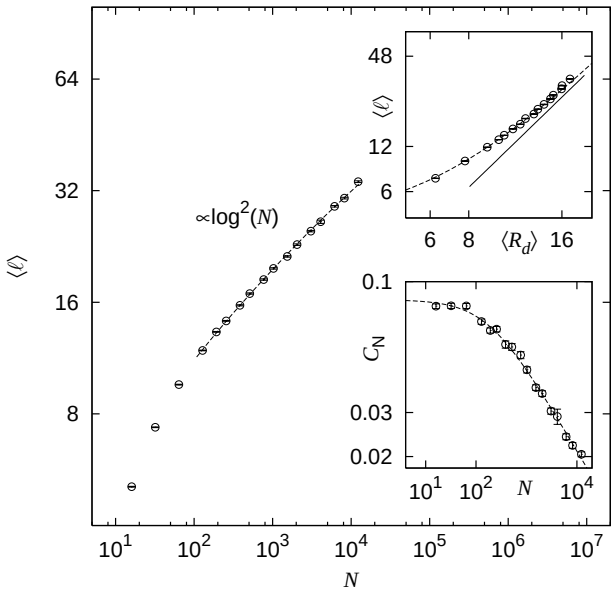

FIG. 7: Scaling behavior of the minimum-weight path length on RRGs respecting a bimodal distribution of the edge-weights at the critcal point $\rho_c = 0.075(2)$. The main plot shows the scaling of the average path length $\langle \ell \rangle$, where the dashed line is a fit to the expression $\langle \ell \rangle \sim \log^2(N)(1 + c/N^d)$. The upper inset illustrates the scaling of $\langle \ell \rangle \sim R_N^2$ and the lower inset shows the scaling of the related finite-size susceptibilty at ρ_c.

C. Scaling at the critical point

We further performed simulations to characterize the scaling behavior of the minimum-weight path length on RRGs respecting a bimodal distribution of the edge-weights at the critcal point $\rho_c = 0.075(2)$, see Fig. 7.

For the average path length $\langle \ell \rangle$, we found a good agreement with the scaling expression $\langle \ell \rangle \sim \log^{d_f}(N) + c_1$. A fit to the data belonging to $N > 100$ yields $d_f = 2.1(1)$ and $c_1 = 5.2(5)$ Considering the scaling expression $\langle \ell \rangle \sim \log^{d_f}(N)(1 + c_1/N^{c_2})$ (main plot of Fig. 7), and taking into account the data belonging to $N > 100$ yields $d_f = 2.3(3)$, $c_1 = 6(3)$ and $c_2 = 0.45(4)$. Fixing $c_2 = 0.5$ improves the result to $d_f = 2.1(1)$ and $c_1 = 6(1)$. Hence, the data for the average path length at ρ_c is in agreement with a scaling exponent $d_f = 2$.

For the NWP problem in finite dimensions we introduced the order parameter $P_\infty = \ell/N$. The respective finite-size suszeptibilities $C_N = N\mathrm{var}(P_\infty) = N^{-1}\mathrm{var}(\ell)$ exhibit the scaling $C_N \sim N^{\gamma/\nu}$ at ρ_c. Here, for the mean-field setup, the latter scaling is modified to $C_N \sim N^{\gamma/\nu^*}$. If we consider corrections to scaling according to $C_N \sim (N + c_1)^{\gamma/\nu^*}$ we yield the estimates $c_1 \approx 180$ and $\gamma/\nu^* = -0.34(2)$ (see lower inset of Fig. 7). The more complicated scaling expression $C_N \sim N^{\gamma/\nu^*}(1 + c_1/N^{c_2})$ yields qualitative similar results, i.e. $\gamma/\nu^* = -0.33(3)$, $c_1 \approx 35$ and $c_2 = 1.0(7)$.

D. Excitations

Next, we want to examine, wether the model exhibits low-energy excitations, which are of order of system size. This would be a numerical evidence that NWP exhibits a complex energy landscape, thus shows "glassy" behavior.

Here, the "size" of an excitation is defined relative to two ground state configurations of loops. I.e., for a given instance of a r-regular random graph G we compute two ground states (GSs) as follows:

(i) Draw a realization of the (bimodal) bond disorder $\omega_{ij}^{(1)}$, $\{i,j\} \in E$, where $|\omega_{ij}^{(1)}| = 1$. Then compute a minimum energy configuration of loops, i.e. GS 1, as explained earlier. The number of loop segments that build up the respective loops is refered to as C_1.

(ii) "Perturb" the realization of disorder according to $\omega_{ij}^{(2)} = \omega_{ij}^{(1)} + \epsilon n_{ij}$, where n_{ij} are independent and identically distributed Gaussian random variables of zero mean and unit variance, and $\epsilon = 1/100$. Compute the corresponding minimum energy configuration, i.e. GS 2, of loops and let C_2 denote the respective number of loop segments.

Now, consider the number $C = |C_2 - C_1|$ of bonds that change by going from GS 1 to GS 2. The average value of C exhibits a scaling of the form $\langle C \rangle = N^\alpha f[(\rho - \rho_c)N^{1/\nu^*}]$, where the choice $\rho_c \approx 0.077$, $\nu^* = 3$ and $\alpha = 0.5$ yields the data collapse illustrated in Fig. 8. Further, the scaling behavior of $\langle C \rangle$ at $\rho_c = 0.077$ is not that clear. However, measurements at $\rho = 0.08 \approx \rho_c$ yield the scaling $\langle C \rangle \sim N^{0.46(4)}$ and at $\rho = 0.32$ they yield $\langle C \rangle \sim N^{0.89(1)}$, as indicated in the inset of Fig. 8. This means that the scaling of the excitation size is weaker than the size of the system. Hence, in the thermodynamic limit, (at least these) low-energy excitations will not cover a finite fraction of the system. These results indicate that the energy landscape of NWP is rather simple, i.e., dominate by one global minimum and close local minima.

IV. ANALYTIC APPROACH: POLYMER IN RANDOM MEDIA

The problem of negative-weight percolation has an interesting correspondence with the problem of polymers in random media. We shall show here that this correspondence can be used to study analytically the percolation threshold on a random graph with a fixed connectivity.

Consider first a closed polymer of length L described by a self-avoiding walk $x = (x_1, \ldots, x_L)$ on the graph G, where $x_i \in V$ are L distinct vertices of G and each pair (x_i, x_{i+1}), as well as (x_L, x_1), belongs to the set of edges E of G. The polymer is subject to a random potential ω on the edges of the graph, so the energy of the polymer is $E_L(x) = \sum_{i=1}^{L} \omega_{x_i, x_{i+1}}$ (we use the notation $x_{L+1} = x_1$).

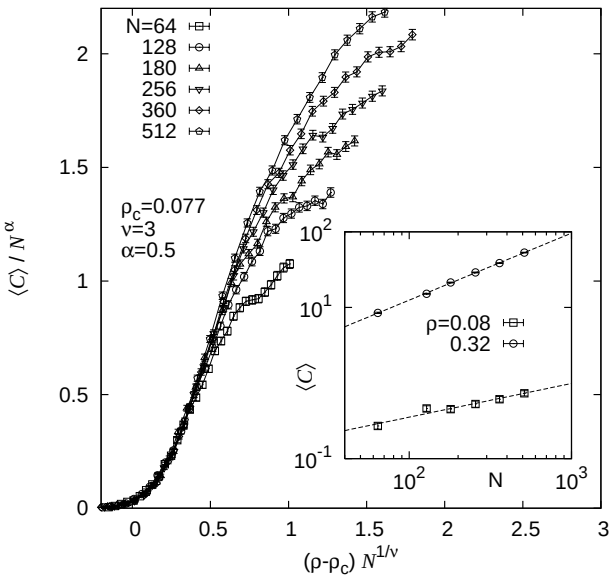

FIG. 8: Scaling behavior of the average number $\langle C\rangle$ of bonds that change upon perturbing the ground state configuration of loops, as explained in the text. The main plot shows the scaled data and the inset shows the scaling of $\langle C\rangle$ as a function of the system size N.

We suppose that the values of ω on the edges are iid quenched random variables drawn from the distribution $P(\omega)$ given by Eq. (1).

We consider now a gas of such polymers, mutually avoiding, and we denote by M the total number of polymers present in the system. We study this problem at equilibrium in a grand-canonical ensemble in which the inverse temperature is equal to β and the chemical potential is equal to μ. Note that in the remainder of this section, the inverse temperature is denoted by β. In order not to confuse it with the order parameter exponent introduced previously in Eq. (6), the latter one will be referred to as *critical exponent* β in the remainder of this subsection. The partition function describing this system is

$$Z = \sum_{M=0}^{\infty} e^{\beta\mu M} \sum_{\{x\}} e^{-\beta E_M(x)} \ , \qquad (7)$$

where $E_M = \sum_n E_{L_n}$ is the total energy of the various polymers of lengths $L_1, L_2, \ldots$.

A similar description of polymers in a solvent has been introduced already in [39]. The study of homopolymers (without disorder), shows that, in order to describe free polymers (in equilibrium with the solvent) the chemical potential has to be adjusted to a critical value μ_c. This critical value corresponds to a phase transition between an infinitely diluted phase for $\mu < \mu_c$ and a dense phase with $\langle M\rangle/N > 0$ (and a non-vanishing osmotic pressure) for $\mu > \mu_c$. From Eq. (7), one finds that μ_c is equal to the canonical free energy density of a gas of polymers: $\mu_c = -(1/(\beta M))\log(\sum_{\{x\}} e^{-\beta E_M(x)})$. If the phase transition is continuous the density on the coexistence line vanishes. Studies of interacting heteropolymers have confirmed this statement [40, 41]. We shall therefore develop a formalism allowing to compute the average density of monomers on a point, ψ, as function of the inverse temperature β, the chemical potential μ and the amount of disorder ρ. For fixed value of β and ρ, the critical chemical potential μ is obtained as the largest value of μ where $\psi = 0$.

We conjecture that this problem of polymer in random medium is equivalent to the NWP problem in the following sense. The set of polymers defines the loops of NWP. Taking the zero temperature ($\beta \to \infty$) limit, one can study if the ground-state energy of the set of polymers is negative (then the corresponding polymer configuration is an admissible NWP), or not. The phase transition of NWP then describes a transition between a 'percolating' phase where the density ψ of the ground state is positive, and a non-percolating phase where it vanishes. Within our conjecture, we can thus study the NWP phase transition as follows: we should find the ground state of the polymer, at $\mu = \mu_c = 0$: the condition $\mu = \mu_c$ allows to study the polymer at equilibrium, the condition $\mu_c = 0$ finds the critical point of NWP where the ground state energy vanishes. We formulate this equivalence between NWP and polymers as a conjecture for the following reason. In the polymer approach we request that the energy of the full set of polymers be negative, while NWP requests that each individual polymer have negative energy. considering the thermodynamic limit where the length of the polymers is large, and the fact that on a random regular graph almost all loops are large since the typical size of closed circuits on such a graph scale like $\log(N)$, it is reasonable to assume that the distribution of energies of each polymer will follow a large deviation principle, so that the request of negative energy for the full set should be equivalent to the request of negative energy for each polymer.

We shall see below that the analytic solution of the polymer problem with the cavity method is in good agreement with the numerical results on the NWP. These results suggest that the conjecture is correct, and that the NWP can be studied analytically through this correspondence with polymers.

The polymer problem can be studied using the cavity method as developed in [40, 41]. Here, we shall use only the replica symmetric cavity method as we have not found any evidence for sizeable replica symmetry breaking effects. This is justified also by the results for the low-energy excitations presented in section III D. We consider a vertex i, we denote by ∂i the set of vertices which are connected to i by an edge, and we study the cavity graph in which one edge $\{i, j\}$ (with $j \in \partial i$) has been removed. We consider the probabilities of the three possible configurations of site i, as shown in Fig. 9.

- The probability that there is no polymer on i is

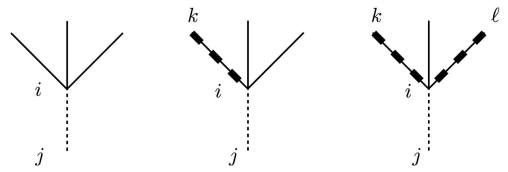

FIG. 9: In a cavity graph where the edge (ij) has been removed, there are three possible conformations of a polymer on site i. Left: no polymer. The probability of these configurations is $p^{(0)}_{i\to j}$. Center: The polymer arrives on i from some other site k (and will be forced to continue on the edge (ij) when this edge will be put back in the graph). The probability of these configurations is $p^{(1)}_{i\to j}$. Right: The polymer goes through i, connecting two sites k and ℓ. The probability of these configurations is $p^{(2)}_{i\to j}$.

denoted $p^{(0)}_{i\to j}$.

- The probability that there is a polymer arriving on i from one edge connecting i to a vertex $k \in \partial i \setminus j$ (meaning that it will be forced to use the edge $\{i, j\}$). This probability is denoted $p^{(1)}_{i\to j}$.

- The probability that the polymer goes through i and uses two edges connecting i to two vertices k, ℓ in $\partial i \setminus j$. It is denoted $p^{(2)}_{i\to j}$.

The random regular graph is locally tree-like, which means that the environment up to any finite distance from a generic point is a regular tree. Using this property, which justifies the fact that random variables on different branches of the cavity graph are independent (within the replica symmetric hypothesis [42]), one can show that these probabilities satisfy the following recursion rules:

$$\begin{aligned} p^{(0)}_{i\to j} &= C \prod_{m\in\partial i\setminus j} (p^{(0)}_{m\to i} + p^{(2)}_{m\to i}) \\ p^{(1)}_{i\to j} &= Ce^{\beta\mu} \sum_{k\in\partial i\setminus j} p^{(1)}_{k\to i} e^{-\beta\omega_{ki}} \prod_{m\in\partial i\setminus j,k} (p^{(0)}_{m\to i} + p^{(2)}_{m\to i}) \\ p^{(2)}_{i\to j} &= Ce^{\beta\mu} \sum_{k<\ell\in\partial i\setminus j} p^{(1)}_{k\to i} e^{-\beta\omega_{ki}} p^{(1)}_{\ell\to i} e^{-\beta\omega_{\ell i}} \\ &\quad \prod_{m\in\partial i\setminus j,k,\ell} (p^{(0)}_{m\to i} + p^{(2)}_{m\to i}) \ . \end{aligned} \tag{8}$$

The constant C is a normalization constant, it is fixed by the condition $p^{(0)}_{i\to j} + p^{(1)}_{i\to j} + p^{(2)}_{i\to j} = 1$. The knowledge of the cavity probabilities $p^{(0)}_{i\to j}, p^{(1)}_{i\to j}, p^{(2)}_{i\to j}$ allows to obtain the various physical quantities. For instance, the probability ψ_i that site i is visited by a polymer is given by

$$\psi_i = \frac{N_i}{D_i} \ , \tag{9}$$

where

$$N_i = e^{\beta\mu} \sum_{k<\ell\in\partial i} p^{(1)}_{k\to i} e^{-\beta\omega_{ki}} p^{(1)}_{\ell\to i} e^{-\beta\omega_{\ell i}} \tag{10}$$

$$\prod_{m\in\partial i\setminus k,\ell} (p^{(0)}_{m\to i} + p^{(2)}_{m\to i}) \ , \tag{11}$$

and

$$D_i = \prod_{m\in\partial i} (p^{(0)}_{m\to i} + p^{(2)}_{m\to i}) + N_i \ . \tag{12}$$

It is possible to simplify the equations by a change of variables. Let us introduce

$$h_{ij} \equiv h_{i\to j} = \frac{1}{\beta} \log \frac{p^{(1)}_{i\to j}}{p^{(0)}_{i\to j} + p^{(2)}_{i\to j}} \ . \tag{13}$$

One can write the cavity equations in terms only of the fields $h_{i\to j}$:

$$h_{i\to j} = \frac{1}{\beta} \log \frac{e^{\beta\mu} \sum_{k\in\partial i\setminus j} e^{\beta(h_{ki}-\omega_{ki})}}{1 + e^{\beta\mu} \sum_{k<\ell\in\partial i\setminus j} e^{\beta(h_{ki}-\omega_{ki}+h_{\ell i}-\omega_{\ell i})}} \tag{14}$$

These equations can be solved by iteration, and their solution gives access to various properties of the polymer. The probability that a given site i is occupied is given by

$$\psi_i = \frac{e^{\beta\mu} \sum_{k<\ell\in\partial i} e^{\beta(h_{ki}-\omega_{ki}+h_{\ell i}-\omega_{\ell i})}}{1 + e^{\beta\mu} \sum_{k<\ell\in\partial i} e^{\beta(h_{ki}-\omega_{ki}+h_{\ell i}-\omega_{\ell i})}} \ , \tag{15}$$

and the probability that the edge (ij) is occupied is given by

$$\psi_{(ij)} = \frac{e^{\beta(h_{ij}+h_{ji}-\omega_{ij})}}{1 + e^{\beta(h_{ij}+h_{ji}-\omega_{ij})}} \ . \tag{16}$$

The above equations allow for the study of one given instance of the problem, i.e. one given realisation of the random graph and of the potential. In the thermodynamic limit, average properties like the average site density $\psi = \frac{1}{N}\sum_i \psi_i$ are self-averaging (their fluctuations from sample to sample go to zero in the large N limit). These self-averaging properties can be studied using the distribution of cavity fields $Q(h)$, which is the probability density that the field $h_{i\to j}$ on an edge $(ij) \in \mathcal{E}$ chosen at random uniformly in a randomly chosen sample is equal to h. The cavity Eqs. (14) imply that $Q(h)$ satisfies the integral equation:

$$\begin{aligned} Q(h) &= \int \prod_{n=1}^{K} [Q(h_n) dh_n P(\omega_n) d\omega_n] \\ &\quad \delta \left(h - \frac{1}{\beta} \log \frac{e^{\beta\mu} \sum_n e^{\beta(h_n-\omega_n)}}{1 + e^{\beta\mu} \sum_{m<n} e^{\beta(h_m-\omega_m+h_n-\omega_n)}} \right) \ , \end{aligned} \tag{17}$$

where $K = r - 1$ is the number of neighbours of the root site in the cavity graph, and the indices m and n run from 1 to K. This integral equation can be solved

efficiently by the numerical approach of 'population dynamics' described in [43]. The average density is then obtained as:

$$\psi = \int \prod_{n=1}^{r} [Q(h_n) dh_n P(\omega_n) d\omega_n] \frac{e^{\beta\mu} \sum_{k<\ell} e^{\beta(h_k - \omega_k + h_\ell - \omega_\ell)}}{1 + e^{\beta\mu} \sum_{k<\ell} e^{\beta(h_k - \omega_k + h_\ell - \omega_\ell)}} \ . \quad (18)$$

We have used this approach to study the polymer at zero temperature (using the infinite β limit of the Eqs. (17),(18)) which is are easily written. Fig. 10 shows the average density computed by solving Eq. (17) for $Q(h)$ with the population dynamics, and using the resulting probability density in Eq. (18). The data shows that, for a given strength of disorder ρ, the average density ψ vanishes at a critical value $\mu_c(\rho)$ of the chemical potential μ, with a quadratic behaviour:

$$\psi \simeq A(\mu - \mu_c(\rho))^2 \ . \quad (19)$$

According to our above conjecture, the critical value ρ_c of the disorder strength is obtained when the corresponding chemical potential vanishes: $\mu_c(\rho_c) = 0$. With this method one obtains the prediction $\rho_c = 0.072 \pm 0.002$. One also sees from Fig. 10, by observing the shift of the curves when changeing the value of ρ, that $\mu_c(\rho)$ has a linear dependence on ρ when $\rho \to \rho_c$:

$$\mu_c(\rho) \simeq B(\rho - \rho_c) \ . \quad (20)$$

Combining Eqs. (19) and (20) shows that the density of the polymer at zero chemical potential grows quadratically when $\rho > \rho_c$: $\psi(\mu = 0) = AB^2(\rho - \rho_c)^2$. This can also be seen directly by studying the $\mu = 0$ case explicitly, see the inset of Fig. 10. This gives according to Eq. (6) the value of the orderparameter exponent $\beta = 2$.

These results show a good agreement between the analytical and numerical approaches both for the value of ρ_c and for the value of the critical exponent β.

V. CONCLUSIONS

We have presented an analytical and a numerical study of the NWP problem in a mean-field case. The analytical study is based on a conjectured equivalence with the problem of SAWs in random medium. The numerical study is based on a mapping to a minimum-weight matching problem for which fast algorithms exist. Both approaches yield results which are in agreement, on the location of the phase transition, on the value of critical exponents, and on the absence of any sizeable indications of a glass phase: this is seen analytically in the fact that we do not find any spin glass instability, and in the numerical study from the sub-extensive scaling of the size of low-lying exitations. It is interesting to note that the simulations of NWP using the minimum-weight matching turn out to be a very efficient numerical approach to the difficult problem of polymers in random media.

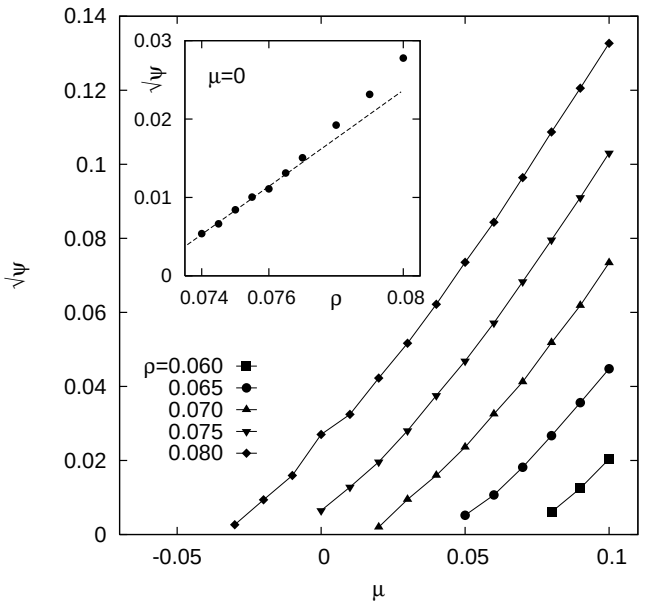

FIG. 10: The average density of the polymer at $\beta = \infty$ has been computed by solving Eq. (17) for $Q(h)$ with the population dynamics method, with a population size of 100000 fields, and using the resulting probability density in Eq. (18). The plot shows $\sqrt{\psi}$ as function of the chemical potential μ. The various curves correspond to different values of the strength of disorder ρ: from right to left, $\rho = 0.06, 0.065, \ldots, 0.080$. The inset shows $\sqrt{\psi}$ versus ρ for $\mu = 0$.

To conclude, we summarize the numerical results found for the scaling exponents of NWP on regular random graphs with fixed connectivity $r = 3$:

$$\text{RRGs}: \quad \nu^* = 3.0(1) \qquad \beta = 2.0(1)$$
$$d_f = 2.1(1) \qquad \gamma = -1.02(2) \, .$$

These agree within error bars with the results found previously [22] for the NWP problem on $6d$ hypercubic lattice graphs:

$$6d: \quad d\nu = 3.00(1) \qquad \beta = 1.92(6)$$
$$d_f = 2.00(1) \qquad \gamma = -0.99(3) \, .$$

These results further support an upper critical dimension $d_u = 6$ for the NWP problem.

Via these and previous results, the static behavior of ordinary NWP is now rather well understood. Since the NWP allows for a very efficient numerical treatment, it would be quite rewarding to study NWP on directed graphs or NWP on systems exhibiting correlated disorder. Also it could be interesting to study the dynamic behavior using local stochastic algorithms while comparing to the exact equilibrium behavior.

Acknowledgments

MM thanks the Humboldt foundation for its support, and the University of Oldenburg for its hospitality. OM acknowledges financial support from the DFG (*Deutsche Forschungsgemeinschaft*) under grant HA3169/3-1. The simulations were performed at the GOLEM I cluster for scientific computing at the University of Oldenburg (Germany). AKH thanks the LPTMS, Université Paris Sud (Orsay) for its hospitality and financial support.

[1] M. Kardar and Y. C. Zhang, Phys. Rev. Lett. **58**, 2087 (1987).
[2] B. Derrida, Physica A **163**, 71 (1990).
[3] P. Grassberger, J. Phys. A **26**, 1023 (1993).
[4] S. V. Buldyrev, S. Havlin, and H. E. Stanley, Phys. Rev. E **73** (2006).
[5] F. O. Pfeiffer and H. Rieger, J. Phys.: Condens. Matter **14**, 2361 (2002).
[6] F. O. Pfeiffer and H. Rieger, Phys. Rev. **E 67**, 056113 (2003).
[7] T. Vachaspati and A. Vilenkin, Phys. Rev. D **30**, 2036 (1984).
[8] R. J. Scherrer and J. A. Frieman, Phys. Rev. D **33** (1986).
[9] H. Hindmarsch and K. Strobl, Nucl. Phys. **B 437**, 471 (1995).
[10] M. Cieplak, A. Maritan, and J. R. Banavar, Phys. Rev. Lett. **72**, 2320 (1994).
[11] O. Melchert and A. K. Hartmann, Phys. Rev. B **76**, 174411 (2007).
[12] K. Schwarz, A. Karrenbauer, G. Schehr, and H. Rieger, J. Stat. Mech. **2009**, P08022 (2009).
[13] N. Schwartz, A. L. Nazaryev, and S. Havlin, Phys. Rev. E **58**, 7642 (1998).
[14] H. Rieger, J. Phys. A **36** (2003).
[15] A. K. Hartmann, in *Rugged Free Energy Landscapes*, edited by J. W (Springer, Berlin, 2007), pp. 67 – 106.
[16] D. Stauffer, Phys. Rep. **54**, 1 (1979).
[17] D. Stauffer and A. Aharony, *Introduction to Percolation Theory* (Taylor and Francis, London, 1994).
[18] A. M. Allega, L. A. Fernández, and A. Tarancón, Nucl. Phys. B **332**, 760 (1990).
[19] D. Austin, E. J. Copeland, and R. J. Rivers, Phys. Rev. D **49**, 4089 (1994).
[20] O. Melchert and A. K. Hartmann, New. J. Phys. **10**, 043039 (2008).
[21] L. Apolo, O. Melchert, and A. K. Hartmann, Phys. Rev. E **79**, 031103 (2009).
[22] O. Melchert, L. Apolo, and A. K. Hartmann, Phys. Rev. E **81**, 051108 (2010).
[23] O. Melchert, *PhD thesis* (not published, 2009).
[24] O. Melchert and A. K. Hartmann, Comp. Phys. Comm. **182**, 1828 (2011).
[25] C. K. Thomas and A. A. Middleton, Phys. Rev. B **76**, 220406 (2007).
[26] G. Pardella and F. Liers, Phys. Rev. E **78**, 056705 (2008).
[27] O. Melchert and A. K. Hartmann, Phys. Rev. B **79**, 184402 (2009).
[28] *Papercore* is a free and open access database for summaries of scientific (currently mainly physics) papers., URL `http://www.papercore.org/`.
[29] B. Bollobás and W. F. de la Vega, Combinatorica **2**, 125 (1982).
[30] B. Bollobás, *Random graphs (2nd ed.)* (Cambridge University Press, Cambridge, U.K., 2001).
[31] M. R. Jerrum and S. Skyum, Computers, IEEE Transactions on **C-33**, 190 (1984).
[32] D. Fernholz and V. Ramachandran, Random Structures and Algorithms **31**, 482 (2007).
[33] R. K. Ahuja, T. L. Magnanti, and J. B. Orlin, *Network Flows: Theory, Algorithms, and Applications* (Prentice Hall, 1993).
[34] W. Cook and A. Rohe, INFORMS J. Computing **11**, 138 (1999).
[35] A. K. Hartmann and H. Rieger, *Optimization Algorithms in Physics* (Wiley-VCH, Weinheim, 2001).
[36] For the calculation of minimum-weighted perfect matchings we use Cook and Rohes blossom4 extension to the Concorde library., URL `http://www2.isye.gatech.edu/~wcook/blossom4/`.
[37] T. H. Cormen, C. E. Leiserson, R. L. Rivest, and C. Stein, *Introduction to Algorithms, 2nd edition* (MIT Press, 2001).
[38] A. K. Hartmann, *Practical Guide to Computer Simulations* (World Scientific, Singapore, 2009).
[39] P. G. de Gennes, J. Phys. Lett. (Paris) **36**, L55 (1975).
[40] M. Mueller, M. Mézard, and A. Montanari, Phys. Rev. Lett. **92**, 185509 (2004).
[41] M. Mueller, M. Mézard, and A. Montanari, J. Chem. Phys. **120**, 11233 (2004).
[42] M. Mézard and A. Montanari, *Information, Physics, and Computation* (Oxford University Press, Oxford, U.K., 2009).
[43] M. Mézard and G. Parisi, Eur. Phys. J. B **20**, 217 (2001).